

# EXPERIMENTAL VALIDATION OF THE NF–FF TRANSFORMATION WITH HELICOIDAL SCANNING SUITABLE FOR ELONGATED ANTENNAS

F. D’Agostino <sup>(1)</sup>, F. Ferrara <sup>(1)</sup>, C. Gennarelli <sup>(1)</sup>, R. Guerriero <sup>(1)</sup>, J.A. Fordham <sup>(2)</sup>,  
M. Migliozi <sup>(1)</sup>, C. Rizzo <sup>(3)</sup>

- (1) D.I.I.I.E. - University of Salerno, via Ponte Don Melillo, 84084 Fisciano (SA), Italy.  
(2) MI Technologies, 1125 Satellite Blvd, Suite 100 Suwanee, Georgia 30024-4629, USA  
(3) MI Technologies Europe, 3 Hither Green Southbourne Emsworth, PO10 8JA, UK.

## ABSTRACT

In this work an experimental validation of the near-field – far-field transformation technique with helicoidal scanning tailored for elongated antennas is provided. Such a transformation relies on the theoretical results relevant to the nonredundant sampling representations of the electromagnetic fields and makes use of an optimal sampling interpolation algorithm, which allows the reconstruction of the near-field data needed by the near-field – far-field transformation with cylindrical scan. In such a case, a prolate ellipsoid is employed to model an elongated antenna, instead of the sphere adopted in the previous approach. It is so possible to consider measurement cylinders with a diameter smaller than the source height, thus reducing the error related to the truncation of the scanning surface. The comparison of the reconstructions obtained from the data directly measured on the classical cylindrical grid with those recovered from the nonredundant measurements on the helix assesses the validity of this innovative scanning technique.

**Keywords:** Near-field – far-field transformation techniques, Helicoidal scanning, Nonredundant sampling representations of electromagnetic fields, Ellipsoidal source modelling.

## 1. Introduction

When far-field (FF) range size limitations, transportation and mounting problems make impossible or impractical the measurement of the radiation patterns on a conventional FF range, it is convenient to exploit near-field (NF) measurements to recover the FF patterns via NF–FF transformation techniques [1-4]. The NF measurements may be performed in a controlled environment, as an indoor shielded anechoic chamber, which allows one to overcome those drawbacks that, due to weather conditions (rain, snow, etc.), electromagnetic (EM) interference and other, cannot be eliminated in FF measurements. The reduction of the time required for the acquisition of the NF data is a very important issue for the antenna

measurement community. As a matter of fact, such a time is currently very much greater than that needed to carry out the corresponding NF–FF transformation. In order to satisfy this demand, the use of the modulated scattering technique employing arrays of scattering probes, which allows a very fast electronic scanning, has been proposed in [5]. However, antenna testing NF facilities based on such a technique are not very flexible. When using mechanical scans, the time reduction requirement can be accomplished, as suggested by Rahmat-Samii et alii in [6], by employing continuous and synchronized movements of the positioning systems of the probe and antenna under test (AUT). Accordingly, innovative NF–FF transformation techniques from a nonredundant number of data collected along spirals wrapping the conventional scanning surfaces have been recently developed [7-10]. In particular, an effective NF–FF transformation with helicoidal scanning has been proposed in [7, 10], by applying the theoretical results on the nonredundant sampling representations of EM fields [11] and assuming the AUT as enclosed in a sphere of radius  $a$ . This target has been achieved: a) by developing a nonredundant sampling representation of the voltage on the helix; b) by choosing the step of such a curve equal to the sample spacing required to interpolate the data along a generatrix. This allows the recovering of the NF data required by the standard probe compensated NF–FF transformation technique with cylindrical scanning [12].

However, the use of the spherical AUT modelling does not permit to consider measurement cylinders having diameter less than the antenna maximum size. This drawback is particularly heavy when dealing with elongated antennas, since it gives rise to an increase of the error related to the truncation of the scanning surface. As a matter of fact, for a given size of the scan zone, such an error raises on increasing the radius of the measurement cylinder. In addition, for this kind of antennas, the redundancy of the spherical modelling reflects in a useless growth of the NF data number. To overcome these drawbacks, an

efficient probe compensated NF–FF transformation technique with helicoidal scanning, which uses a prolate ellipsoidal source modelling tailored for elongated antennas (see Fig. 1), has been developed in [13].

The aim of this work is to provide its experimental validation, which is carried out at the laboratory of antenna characterization of the University of Salerno, where an advanced cylindrical NF measurement facility is available. The comparison between the reconstructions obtained from the data directly measured on the classical cylindrical grid and those recovered from nonredundant measurements acquired on the helix will show that the helicoidal scanning retains the accuracy of the classical cylindrical approach and allows one to remarkably reduce the time required for the data acquisition.

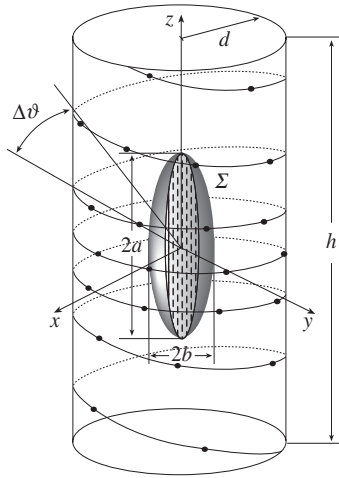


**Figure 1** - Helicoidal scan for an elongated AUT.

## 2. Helicoidal scan for an elongated AUT

The main results [13] concerning the reconstruction of the voltage from the knowledge of a nonredundant number of its samples collected by the measurement probe along a helix are here summarized for reader's convenience.

Let us consider an AUT and a non directive probe scanning a proper helix lying on a cylinder of radius  $d$  (see Fig. 1) and adopt the spherical coordinate system  $(r, \vartheta, \phi)$  for denoting the observation point  $P$ . Since the voltage  $V$  measured by such a probe has the same effective spatial bandwidth of the field, the theoretical results relevant to the nonredundant representation of EM fields [11] can be applied to it. Accordingly, if the AUT is enclosed in a convex domain bounded by a surface  $\Sigma$  with rotational symmetry and the observation curve is described by a proper analytical parameterization  $\underline{r} = \underline{r}(\xi)$ , it is convenient to introduce the probe “reduced voltage”

$$\tilde{V}(\eta) = V(\eta) e^{j\psi(\eta)} \quad (1)$$

where  $\psi(\eta)$  is a phase function to be determined. The bandlimitation error, occurring when the reduced voltage is approximated by a bandlimited function, becomes negligible as the bandwidth exceeds a critical value  $W_\eta$  [11]. Therefore, such an error can be effectively controlled by choosing a bandwidth equal to  $\chi' W_\eta$ ,  $\chi'$  being an excess bandwidth factor slightly greater than unity for an electrically large AUT.

As shown in [13], a two-dimensional optimal sampling interpolation (OSI) algorithm to reconstruct the voltage from a nonredundant number of its samples collected by the probe along a helix can be obtained by developing a nonredundant sampling representation of the voltage on a helix, whose step must be chosen equal to the sample spacing required to interpolate the data along a generatrix.

When considering an elongated AUT, it is convenient to choose the surface  $\Sigma$  coincident with the smallest prolate ellipsoid having major and minor semi-axes equal to  $a$  and  $b$  (Fig. 1). In such a case, by adopting  $W_\eta = \beta \ell' / 2\pi$  ( $\beta$  being the wavenumber and  $\ell'$  the length of the intersection curve  $C'$  between the meridian plane through  $P$  and the ellipsoid), the expressions for the phase function  $\psi$  and the parameterization  $\eta$  to be used for describing a generatrix are [11]:

$$\psi = \beta a \left[ v \sqrt{\frac{(v^2 - 1)}{(v^2 - \varepsilon^2)}} - E \left( \cos^{-1} \sqrt{\frac{(1 - \varepsilon^2)}{(v^2 - \varepsilon^2)}} \middle| \varepsilon^2 \right) \right] \quad (2)$$

$$\eta = (\pi/2) \left[ 1 + E(\sin^{-1} u | \varepsilon^2) / E(\pi/2 | \varepsilon^2) \right] \quad (3)$$

where  $u = (r_1 - r_2) / 2f$  and  $v = (r_1 + r_2) / 2a$  are the elliptic coordinates,  $r_{1,2}$  being the distances from  $P$  to the foci and  $2f$  the focal distance of  $C'$ . Moreover,  $\varepsilon = f/a$  is the eccentricity of  $C'$ , and  $E(\cdot | \cdot)$  denotes the elliptic integral of second kind. It is worth noting that in any meridian plane the curves  $\psi = \text{const}$  and  $\eta = \text{const}$  are ellipses and hyperbolas confocal to  $C'$  (Fig. 2), instead of circumferences and radial lines, as in the spherical modelling case.

The parametric equations of the helix, when imposing its passage through a fixed point  $P_0$  of the generatrix at  $\phi = 0$ , are:

$$\begin{cases} x = d \cos(\phi - \phi_i) \\ y = d \sin(\phi - \phi_i) \\ z = d \cot[\vartheta(\eta)] \end{cases} \quad (4)$$

wherein  $\phi$  is the angular parameter describing the helix,  $\phi_i$  is the value of  $\phi$  at  $P_0$ , and  $\eta = k\phi$ . Such a helix is obtained as projection of a proper spiral wrapping the surface  $\Sigma$  modelling the AUT on the scanning cylinder by means of the curves at  $\eta = \text{const}$

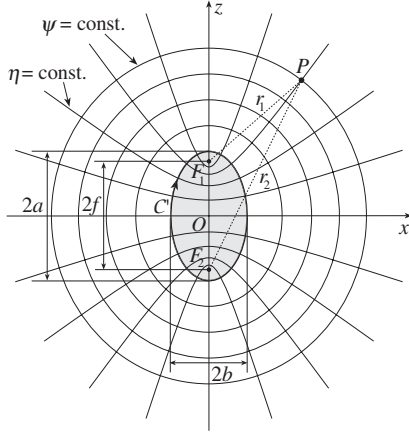


**Figure 2** - Ellipsoidal source modelling.

[13]. The parameter  $k$  is such that the step of this spiral, determined by the consecutive intersections  $Q(\phi)$  and  $Q(\phi+2\pi)$ , is chosen equal to the sample spacing  $\Delta\eta = 2\pi/(2N''+1)$ , where  $N'' = \text{Int}(\chi N') + 1$ , being  $N' = \text{Int}(\chi' W_\xi) + 1$ . As a consequence, being  $\Delta\eta = 2\pi k$ , it follows that  $k = 1/(2N''+1)$ . The function  $\text{Int}(x)$  gives the integer part of  $x$  and  $\chi > 1$  is an oversampling factor needed for controlling the truncation error.

The phase function and the parameterization to be used for obtaining a nonredundant sampling representation along the helix can be determined according to a heuristic reasoning [13]. In particular, by generalizing the corresponding relations relevant to the spherical AUT modelling case, the phase function  $\gamma$  coincides with  $\psi$  defined in (2), and the parameter  $\xi$  is  $\beta/W_\xi$  times the curvilinear abscissa of the projecting point that lies on the spiral wrapping the ellipsoid. Moreover, according to [13],  $W_\xi$  is chosen to be equal to  $\beta/\pi$  times the length of the spiral wrapping the ellipsoid from pole to pole. Namely, the spiral,  $\gamma$  and  $\xi$  are such that they coincide with those relevant to the spherical modelling, when the prolate ellipsoid leads to a sphere.

According to these results, the OSI formula to reconstruct the voltage at any point  $Q$  of the helix is [11]:

$$\tilde{V}(\xi) = \sum_{m=m_0-p+1}^{m_0+p} \tilde{V}(\xi_m) \Omega_M(\xi - \xi_m) D_{M''}(\xi - \xi_m) \quad (5)$$

where  $m_0 = \text{Int}[(\xi - \xi(\phi_i))/\Delta\xi]$  is the index of the sample nearest (on the left) to the output point,  $2p$  is the number of retained samples  $\tilde{V}(\xi_m)$ , and

$$\xi_m = \xi(\phi_i) + m\Delta\xi = \xi(\phi_i) + 2\pi m/(2M''+1) \quad (6)$$

with  $M'' = \text{Int}(\chi M') + 1$  and  $M' = \text{Int}(\chi' W_\xi) + 1$ . Moreover,

$$D_{M''}(\xi) = \frac{\sin((2M''+1)\xi/2)}{(2M''+1) \sin(\xi/2)} \quad (7)$$

$$\Omega_M(\xi) = \frac{T_M[-1 + 2(\cos(\xi/2)/\cos(\bar{\xi}/2))^2]}{T_M[-1 + 2/\cos^2(\bar{\xi}/2)]} \quad (8)$$

are the Dirichlet and Tschebyscheff Sampling functions, wherein  $T_M(\xi)$  is the Tschebyscheff polynomial of degree  $M = M'' - M'$  and  $\bar{\xi} = p\Delta\xi$ .

The OSI formula (5) can be used to evaluate the “intermediate samples”, namely, the voltage values at the intersection points between the helix and the generatrix passing through  $P$ . Once these samples have been evaluated, the NF data required by the NF-FF transformation technique [12] can be reconstructed via the following OSI expansion:

$$\tilde{V}(\eta(\vartheta), \varphi) = \sum_{n=n_0-q+1}^{n_0+q} \tilde{V}(\eta_n) \Omega_N(\eta - \eta_n) D_{N''}(\eta - \eta_n) \quad (9)$$

where  $n_0 = \text{Int}[(\eta - \eta_0)/\Delta\eta]$ ,  $\tilde{V}(\eta_n)$  are the voltage intermediate samples,

$$\eta_n = \eta_n(\varphi) = \eta(\phi_i) + k\varphi + n\Delta\eta = \eta_0 + n\Delta\eta \quad (10)$$

and all the other symbols have the same or analogous meaning as in (5).

### 3. Experimental results

The above described approach has been experimentally validated in the anechoic chamber available at the laboratory of antenna characterization of the University of Salerno, which is provided with a NF facility system supplied by MI Technologies. The dimensions of the chamber are  $8\text{ m} \times 5\text{ m} \times 4\text{ m}$ . Pyramidal absorbers are positioned in order to minimize the reflections, thus ensuring a background noise lower than  $-40\text{ dB}$ . The chamber is equipped with a vertical scanner and a rotating table, so that, by properly matching their movements, the NF data can be acquired at any point on a cylindrical surface surrounding the AUT. The vertical scanner has height  $240\text{ cm}$  and is characterized by a linear precision of  $\pm 0.005\text{ cm}$ . The rotating table MI-6111B, mounted with its rotary axis parallel to the vertical scanner, ensures an angular precision of  $\pm 0.05^\circ$ . The controller MI-4190 is used to control the positioners motion. It is completed by the option MI-4193, so that it is able to simultaneously drive both the positioners. Moreover, it is connected to a host computer by means of a IEEE-488 interface. A vectorial network analyzer Anritsu 37247C provides both amplitude and phase measurements with wide dynamic range, high sensitivity and linearity over the range from  $40\text{ MHz}$  to  $20\text{ GHz}$ . It is computer-

controlled and is connected to both the probe and the AUT. An open-ended MI-6970-WR90 rectangular waveguide, whose end is tapered for minimizing the diffraction effects, is used as probe. The AUT, located in the plane  $x = 0$ , is a resonant slotted waveguide array 37.7 cm long, fed at the center of the bottom broad wall by a coaxial line, operating at 10 GHz. It has been obtained from a WR-90 waveguide by cutting in it two rows each of  $N = 10$  round-ended slots. These rows are at the same distance from the center line of the broad waveguide wall. The slots are longitudinally directed and uniformly spaced by  $\lambda_g/2$ , wherein  $\lambda_g$  is the guide wavelength. According to the described sampling representation, the AUT has been modelled as enclosed in a prolate ellipsoid with major and minor semi-axes equal to 21 cm and 4.2 cm. The output probe voltages have been collected on a helix lying on a cylinder having  $d = 18$  cm and  $h = 230.85$  cm. To assess the effectiveness of the two-dimensional OSI algorithm, the amplitudes of the reconstructed probe voltage relevant to the generatrices at  $\varphi = 0^\circ$  and  $\varphi = 30^\circ$  are compared in Figs. 3 and 4 with those directly measured on the same generatrices. As can be seen, there is an excel-

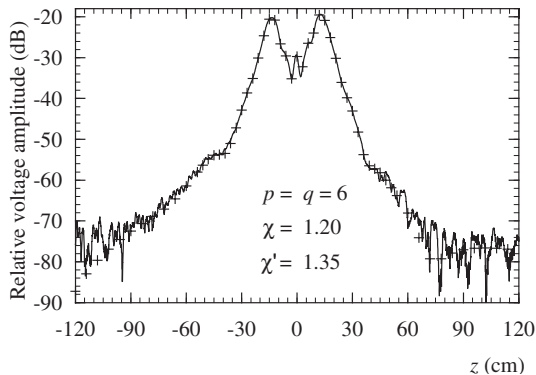


**Figure 3** - Amplitude of the probe voltage on the generatrix at  $\varphi = 0^\circ$ . Solid line: measured. Crosses: interpolated.

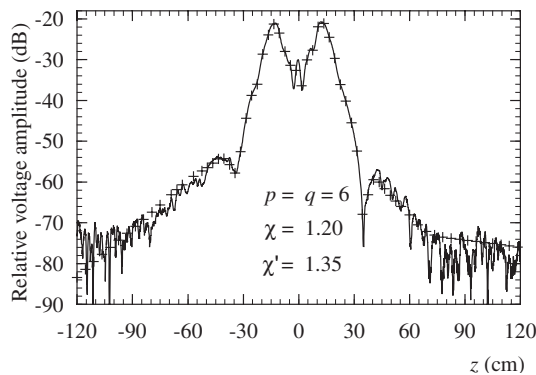


**Figure 4** - Amplitude of the probe voltage on the generatrix at  $\varphi = 30^\circ$ . Solid line: measured. Crosses: interpolated.

lent agreement between the reconstructed voltage (crosses) and the measured one (solid line), save for the peripheral zone (below about  $-60$  dB), wherein the error is caused both by the truncation of the scanning zone and the environmental reflections. Note that, due to the filtering properties of the interpolation functions, the spatial harmonics relevant to the noise sources outside the AUT spatial bandwidth are cut away. This results in a smoother behaviour of the reconstructed voltage with respect to the measured one. For completeness, the comparison between the phase of the recovered voltage and the measured one on the generatrix at  $\varphi = 0^\circ$  is shown in Fig. 5 only in the range  $[-20$  cm,  $120$  cm] to improve its readability. Note that all the reported reconstructions have been obtained by using  $\chi' = 1.35$ ,  $\chi = 1.20$ , and  $p = q = 6$ .

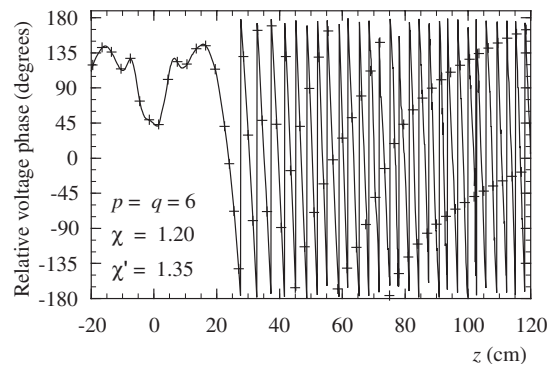


**Figure 5** - Phase of the probe voltage on the generatrix at  $\varphi = 0^\circ$ . Solid line: measured. Crosses: interpolated.

In order to assess the overall effectiveness of the described NF-FF transformation technique, the FF pattern in the principal planes E and H, reconstructed from the acquired helicoidal NF data, is compared in Figs. 6 and 7 with that obtained, by using the software package MI-3000, from the data directly measured on the classical cylindrical grid. The same software has been used to get the FF reconstruction from the helicoidal NF data. To this end, the two-dimensional OSI algorithm has been employed for recovering the cylindrical data needed to perform the NF-FF transformation. As can be seen, in both the planes, there is a very good agreement, thus confirming the effectiveness of the approach.

It is interesting to compare the number of data (1 073) needed by the proposed NF-FF transformation with helicoidal scan with that (5 760) required by traditional cylindrical NF scanning to cover the same scanning zone. As shown, the helicoidal scanning allows one to remarkably reduce the number of measurements, without losing the accuracy of the classical approach. Note that this number is comparable with that (1 285) needed by the nonredundant NF-FF transformation

with cylindrical scanning [14] and is significantly less than that needed by the NF helicoidal scanning technique [15], which requires the same number of the classical cylindrical approach.

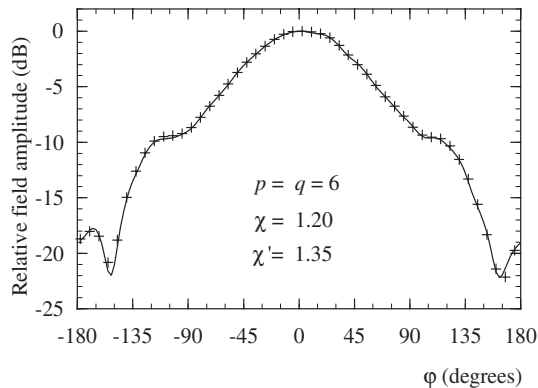


**Figure 6** - E-plane pattern. Solid line: reference. Crosses: reconstructed from NF data acquired via helicoidal scanning.

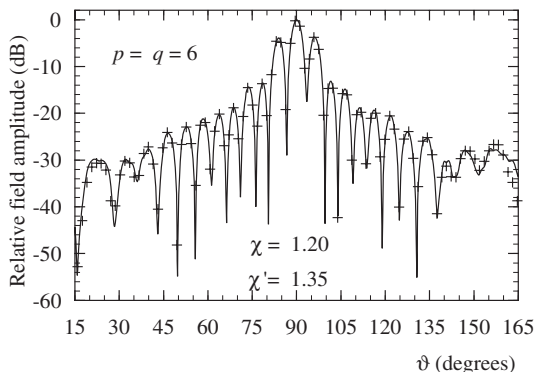


**Figure 7** - H-plane pattern. Solid line: reference. Crosses: reconstructed from NF data acquired via helicoidal scanning.

#### 4. REFERENCES

- [1] "Special Issue on near-field scanning techniques," *IEEE Trans. Antennas Propagat.*, vol. AP-36, pp. 727-901, 1988.
- [2] A.D.Yaghjian, "An overview of near-field antenna measurements," *IEEE Trans. Antennas Propagat.*, vol. AP-34, pp. 30-45, 1986.
- [3] C.Gennarelli, G.Riccio, F.D'Agostino, and F.Ferrara, *Near-field - far-field transformation techniques*, vol. 1, CUES, Salerno, Italy, 2004.
- [4] C.Gennarelli, G.Riccio, F.D'Agostino, F.Ferrara, and R.Guerriero, *Near-field - far-field transformation techniques*, vol. 2, CUES, Salerno, Italy, 2006.
- [5] J. C. Bolomey et alii, "Rapid near-field antenna testing via array of modulated scattering probes," *IEEE Trans. Antennas Propagat.*, vol. AP-36, pp. 804-814, 1988.
- [6] R.G.Yaccarino, L.I.Williams, and Y.Rahmat-Samii, "Linear spiral sampling for the bipolar planar antenna measurement technique," *IEEE Trans. Antennas Propagat.*, vol. AP-44, pp. 1049-1051, 1996.
- [7] O.M.Bucci, C.Gennarelli, G.Riccio, and C.Savarese, "Nonredundant NF-FF transformation with helicoidal scanning," *JEMWA*, vol. 15, pp. 1507-1519, 2001.
- [8] O.M.Bucci, F.D'Agostino, C.Gennarelli, G.Riccio, and C.Savarese, "Probe compensated FF reconstruction by NF planar spiral scanning," *IEE Proc. - Microw., Antennas Propagat.*, vol. 149, pp. 119-123, 2002.
- [9] O.M.Bucci, F.D'Agostino, C.Gennarelli, G.Riccio, and C.Savarese, "NF-FF transformation with spherical spiral scanning," *IEEE Antennas Wireless Propagat. Lett.*, vol. 2, pp. 263-266, 2003.
- [10] F.D'Agostino, C.Gennarelli, G.Riccio, and C.Savarese, "Theoretical foundations of near-field-far-field transformations with spiral scanings," *Progress in Electromagn. Res., PIER 61*, pp. 193-214, 2006.
- [11] O.M.Bucci, C.Gennarelli, and C.Savarese, "Representation of electromagnetic fields over arbitrary surfaces by a finite and nonredundant number of samples," *IEEE Trans. Antennas Propagat.*, vol. 46, pp. 351-359, 1998.
- [12] W.M.Leach Jr. and D.T.Paris, "Probe compensated NF measurements on a cylinder," *IEEE Trans. Antennas Propagat.*, vol. AP-21, pp. 435-445, 1973.
- [13] F.D'Agostino, F.Ferrara, C.Gennarelli, R.Guerriero, and M.Migliozzi, "Near-field - far-field transformation technique with helicoidal scanning for elongated antennas," *Prog. in Electromagn. Res B*, vol. *PIERB 4*, pp. 249-261, 2008.
- [14] F.D'Agostino, F.Ferrara, C.Gennarelli, G.Riccio, and C.Savarese, "NF-FF transformation with cylindrical scanning from a minimum number of data," *Microw. Opt. Technol. Lett.*, vol. 35, pp. 264-270, 2002.
- [15] S.Costanzo and G.Di Massa, "Far-field reconstruction from phaseless near-field data on a cylindrical helix," *J. Electromagn. Waves Appl.*, vol. 18, pp. 1057-1071, 2004.